Article

A Ruler for Determining the Position of Proteins in Membranes

Robert D. Nielsen, Kepeng Che, Michael H. Gelb, and Bruce H. Robinson

J. Am. Chem. Soc., **2005**, 127 (17), 6430-6442• DOI: 10.1021/ja042782s • Publication Date (Web): 08 April 2005

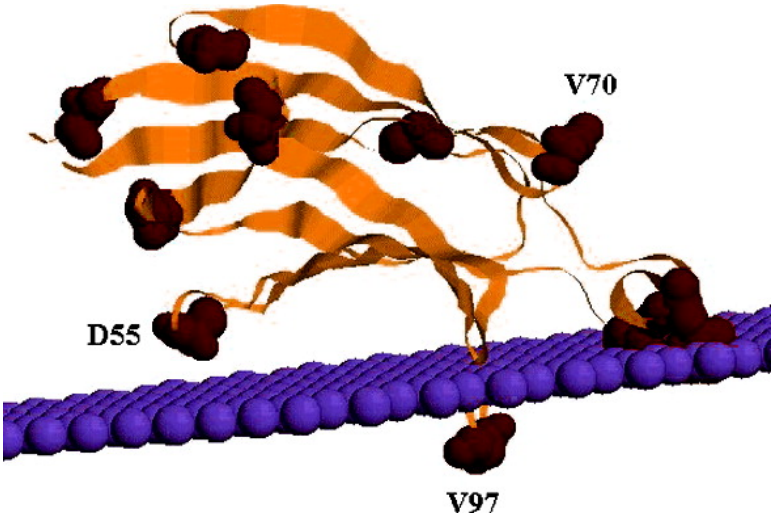

More About This Article

Additional resources and features associated with this article are available within the HTML version:

- Supporting Information
- Links to the 2 articles that cite this article, as of the time of this article download
- Access to high resolution figures
- Links to articles and content related to this article
- Copyright permission to reproduce figures and/or text from this article

View the Full Text HTML

J|A|C|S
ARTICLES
Published on Web 04/08/2005

A Ruler for Determining the Position of Proteins in Membranes

Robert D. Nielsen,[†] Kepeng Che,[†] Michael H. Gelb,*[,†,‡] and Bruce H. Robinson*[,†]

Contribution from the Departments of Chemistry and Biochemistry, University of Washington, Seattle, Washington 98195

Received November 30, 2004; E-mail: robinson@chem.washington.edu; gelb@chem.washington.edu

Abstract: Both the oxygen diffusion rate and the oxygen solubility vary with depth into the interior of biological membranes. The product of these two gradients generates a single gradient, a permeability gradient, which is a smooth continuous function of the distance from the center of the membrane. Using electron paramagnetic resonance and the spin-probe method, the relaxation gradient of oxygen, which is directly proportional to the permeability gradient, is the quantity that can be directly measured in membranes under physiological conditions. The gradient obtained provides a calibrated ruler for determining the membrane depth of residues either from loop regions of membrane-binding proteins or from the membrane-exposed residues of transmembrane proteins. We have determined the relaxation gradient of oxygen in zwitterionic and anionic phospholipid membranes by attaching a single nitroxide probe to a transmembrane α-helical polypeptide at specific residues. The peptide ruler was used to determine the depth of penetration of the calcium-binding loops of the C2 domain of cytosolic phospholipase A_2. The positions of selected residues of this membrane-binding protein that penetrate into the membrane, determined using this ruler, compared favorably with previous determinations using more complex methods. The relaxation gradient constrains the possible values of the membrane-dependent oxygen concentration and the oxygen diffusion gradients. The average oxygen diffusion coefficient is estimated to be at least 2-fold smaller in the membrane than that in water.

Introduction

In situ measurements of the distribution of small molecules, such as oxygen, in biological membranes are important for understanding the structure and dynamics of various lipids and protein−lipid interactions. The measurement of the profiles of such small molecules is difficult to obtain. There now exist a number of techniques, including magnetic resonance, fluorescence quenching, and florescence resonance energy transfer methods,[1−4] to measure the interaction of membrane-soluble molecules with membrane-bound protein. These methods take advantage of the fact that certain molecules of interest, such as oxygen, are also optical quenchers and spin relaxants. One technique, which has been exploited in several contexts to quantify oxygen in membranes, makes use of the fact that oxygen is paramagnetic. While the EPR signal of oxygen is not detectable under standard biological conditions, the presence of oxygen is inferred by collisional interaction with an EPR active probe that is placed in the membrane at known depths. Spin-labeled lipids or lipid analogues, such as spin-labeled *n*-doxyl stearic acid, have been used most frequently as spin probes.[5−10] A spin label, as a doxyl moiety, is introduced at the *n*th carbon positions in the probe lipid, so that the spin label will be sensitive to the oxygen at different depths in the membrane. While spin-labeled lipids and lipid analogous are relatively easy to produce, there are some drawbacks to their use. The spin-labeled lipids are not transmembrane and must incorporate into either the inner or outer leaflet. Furthermore, the lipid probes do not incorporate with perfect order in the membrane. Because the spin-label position on the probe lipid is used to localize the spin label in the membrane, a wide variation in the conformation of the probe lipid complicates interpretation. Disorganization of the probe lipid conformation is expected and has been found as the labeling position nears the center of the membrane bilayer.[11]

An alternative method, introduced to avoid these disadvantages, is the use of spin-labeled transmembrane proteins as a

[†] Department of Chemistry.
[‡] Department of Biochemistry.

(1) Beers, S. A.; Buckland, A. G.; Giles, N.; Gelb, M. H.; Wilton, D. C. *Biochemistry* **2003**, *42*, 7326−7338.
(2) Chattopadhyay, A.; London, E. *Biochemistry* **1987**, *26*, 39−45.
(3) Gambhir, A.; Hangyas-Mihalyne, G.; Zaitseva, I.; Cafiso, D. S.; Wang, J.; Murray, D.; Pentyala, S. N.; Smith, S. O.; McLaughlin, S. *Biophys. J.* **2004**, *86*, 2188−2207.
(4) Luchette, P. A.; Prosser, R. S.; Sanders, C. R. *J. Am. Chem. Soc.* **2002**, *124*, 1778−1781.
(5) Subczynski, W. K.; Hyde, J. S. *Biochim. Biophys. Acta* **1981**, *643*, 283−291.
(6) Subczynski, W. K.; Hyde, J. S. *Biophys. J.* **1984**, *45*, 743−748.
(7) Subczynski, W. K.; Hyde, J. S.; Kusumi, A. *Proc. Natl. Acad. Sci. U.S.A.* **1989**, *86*, 4474−4478.
(8) Subczynski, W. K.; Hyde, J. S.; Kusumi, A. *Biochemistry* **1991**, *30*, 8578−8590.
(9) Subczynski, W. K.; Pasenkiewicz-Gierula, M.; McElhaney, R. N.; Hyde, J. S.; Kusumi, A. *Biochemistry* **2003**, *42*, 3939−3948.
(10) Windrem, D. A.; Plachy, W. Z. *Biochim. Biophys. Acta* **1980**, *600*, 655−665.
(11) Altenbach, C.; Greenhalgh, D. A.; Khorana, H. G.; Hubbell, W. L. *Proc. Natl. Acad. Sci. U.S.A.* **1994**, *91*, 1667−1671.

10.1021/ja042782s CCC: $30.25

probe.[12−14] For example, 10 mutants of bacteriorhodopsin were expressed with cysteine replacing native surface residues on a transmembrane α-helical strand of the protein. The now common MTSSL spin label was attached at the cysteine site of each mutant.[12] Because bacteriorhodopsin is transmembrane and sits in the membrane with known orientation, it does not suffer the same defects as the lipid analogues. The main concern with using the 27 kD bacteriorhodopsin protein is that the spin-labeling sites must be chosen judiciously to avoid steric contact with segments of the protein.[15] In the present study, we spin labeled a single transmembrane α-helical peptide that consists of leucinyl−alanyl repeats capped by terminal tryptophans (WALP).[16] The membrane orientation is well characterized by circular dichroism and IR spectroscopy.[17] The hydrophobic leucinyl−alanyl repeat ensures the peptide is completely inserted in the membrane, and the tryptophans help maintain a consistent registration within the membrane because the tryptophans preferentially partition into the headgroup region of the bilayer.[15,17] Because WALP is a single α-helix, spin labels can be introduced periodically along the WALP peptide. The uniformity of the leucinyl−alanyl repeat in WALP ensures a uniform peptide−spin label orientation. Hence, the range of steric conflicts inevitable when spin labeling a large multi-unit transmembrane protein is avoided.

In early studies of membrane oxygen relaxation, continuous wave EPR spectra were used to measure the collisional interaction of the spin label with oxygen. This was done by measuring the peak-to-peak line width of the standard EPR spectrum to estimate the spin−spin relaxation rate in the presence and absence of oxygen.[10,18,19] The collisional effect of oxygen is to add a new mechanism to spin relaxation and, hence, to increase the rate of relaxation of the spin label. Subsequently, time domain saturation recovery was used to measure the spin−lattice relaxation rate directly in the presence and absence of oxygen.[7,9,20] We use the time domain saturation recovery technique because it is often more accurate than the continuous wave technique for measuring oxygen collisional relaxation.[21]

The collisional effect of oxygen that is measured by EPR depends on the local concentration of oxygen in the vicinity of the spin label. There is additional dependence of the collisional relaxation effect on the relative diffusion of spin label and oxygen.[6] The oxygen collisional relaxation profile depends on the local fluidity of the membrane, through the oxygen diffusion coefficient, which is a transport property and depends on the local viscosity. The conformational freedom of the spin label also depends, in part, on the local fluidity of the membrane. The line width of the continuous wave spectrum is sensitive to spin-label motion and has been used as a semiquantitative measure of spin-label conformational freedom.[22−24] The time domain measured spin−lattice relaxation rate has a monotonic dependence on the degree of spin-label conformational freedom.[21,25] The spin−lattice relaxation rate is measured, as a control, without oxygen. The profile of spin−lattice relaxation rate as a function of position on the WALP peptide in the membrane bilayer is therefore important for corroborating the degree of membrane fluidity and its potential impact on interpretation of the oxygen collisional profile.

The relaxation profile measured herein is proportional to the product of the local concentration of oxygen and the oxygen−nitroxide relative translational diffusion coefficient. For our purposes, it is not necessary to disentangle these two quantities; however, our results provide constraints on these two quantities. The average oxygen concentration in the membrane phase has been inferred from partition coefficients of oxygen in hydrocarbons[10,26] and has also been estimated from proton NMR.[4] Recently, molecular dynamics-based simulations have reached a simulation time scale that allows for prediction of the equilibrium and transport profiles of various small molecules in membrane bilayers as a function of membrane depth.[27,28] These predictions can be tested against experimental equilibrium constants and the experimentally determined relaxation profiles in membrane bilayers[9,10,29] reported herein.

The measurement of the oxygen collisional relaxation profile in membranes is important well beyond the direct biologic implications. Collisional profiles have been used in a secondary role to construct rulers that allow for determination of the depth of insertion into the membrane phase of residues on peripheral membrane proteins.[11] A spin label on a peripheral membrane protein, when inserted into the bilayer, will sense the increased oxygen concentration through the collisional relaxation mechanism.[30,31] When the oxygen relaxation profile has been calibrated (as presented herein), the depth of insertion of the protein residue in the membrane may be quantitatively determined.

Materials and Methods

Purification, Spin Labeling, and Characterization of the Peptides. The WALP peptides were synthesized by SynPep Inc. (Dublin, CA) by manual solid-phase synthesis (peptide names and sequences are given in Table 1). The completion of each coupling was monitored, and multiple couplings were carried out as necessary. Crude peptides were dissolved in trifluoroethanol or methanol, and approximate peptide concentrations were obtained from the absorbance at 280 nm (based on tryptophan). To the peptide solution (3 mg/mL), triethylamine (2 equiv), and MTSSL (1-oxyl-2,2,5,5-tetramethylpyrroline-3-methyl) was

(12) Altenbach, C.; Marti, T.; Khorana, H. G.; Hubbell, W. L. *Science* **1990**, *248*, 1088−1092.
(13) Dzikovski, B. G.; Livshits, V. A.; Marsh, D. *Biophys. J.* **2003**, *85*, 1005−1012.
(14) Perozo, E.; Marien Cortes, D.; Cuello, L. G. *Nat. Struct. Biol.* **1998**, *5*, 459−469.
(15) Killian, J. A. *Biochim. Biophys. Acta* **1998**, *1376*, 401−416.
(16) de Planque, M. R. R.; Goormaghtigh, E.; Greathouse, D. V.; Koeppe, R. E., II; Kruijtzer, J. A. W.; Liskamp, R. M. J.; de Kruijff, B.; Killian, J. A. *Biochemistry* **2001**, *40*, 5000−5010.
(17) Killian, J. A.; Salemink, I.; de Planque, M. R. R.; Lindbloom, G.; Koeppe, R. E., II; Greathouse, D. V. *Biochemistry* **1996**, *35*, 1037−1045.
(18) Hatcher, M. E.; Plachy, W. Z. *Biochim. Biophys. Acta* **1993**, *1149*, 73−78.
(19) Smirnov, A. I.; Belford, R. L. *J. Magn. Reson.* **1995**, *113*, 65−73.
(20) Yin, J.-J.; Hyde, J. S. *Z. Phys. Chem. Neue Folge* **1987**, *153*, 57−65.
(21) Nielsen, R.; Canaan, S.; Gladden, J. A.; Gelb, M. H.; Mailer, C.; Robinson, B. H. *J. Magn. Reson.* **2004**, *169*, 129−163.
(22) Smirnov, A. I.; Clarkson, R. B.; Belford, R. L. *J. Magn. Reson.* **1996**, *B111*, 149−157.
(23) Hubbell, W. L.; Cafiso, D. S.; Altenbach, C. *Nat. Struct. Biol.* **2000**, *7*, 735−739.
(24) Columbus, L.; Hubbell, W. L. *Trends Biochem. Sci.* **2002**, *27*, 288−295.
(25) Robinson, B. H.; Haas, D. A.; Mailer, C. *Science* **1994**, *263*, 490−493.
(26) Wilhelm, E.; Battinon, R. *Chem. Rev.* **1973**, *73*, 1−9.
(27) Marrink, S. J.; Berendsen, J. C. *J. Phys. Chem.* **1996**, *100*, 16729−16738.
(28) Shinoda, W.; Mikami, M.; Baba, T.; Hato, M. *J. Phys. Chem. B* **2004**, *108*, 9346−9356.
(29) Altenbach, C.; Froncisz, W.; Hubbell, W. L. Biophysical Society 46th Annual Meeting, San Francisco, CA. *Biophys. J.* San Francisco, CA, 2002; Vol. 82, p 479a.
(30) Altenbach, C.; Froncisz, W.; Hyde, J. S.; Hubbell, W. L. *Biophys. J.* **1989**, *56*, 1183−1191.
(31) Frazier, A. A.; Wisner, M. A.; Malmberg, N. J.; Victor, K. G.; Fanucci, G. E.; Nalefski, E. A.; Falke, J. J.; Cafiso, D. S. *Biochemistry* **2002**, *41*, 6282−6292.

Table 1. Sequence and Mass Spectrometry Characterization of WALP23 Peptides

position	peptide name	peptide sequence[a]	calcd MW	obsd MW[b]	obsd MW[c]
−2	sl−CAA−WALP23	Ac−C(sl)AAGWWLALALALALALALALALWWA−NH_2	2948		2949, M + H
0	sl−C−WALP23	Ac−C(sl)GWWLALALALALALALALALWWA−NH_2	2806		2807, M + H
1	sl−WALP23−C1	Ac−C(sl)WWLALALALALALALALALWWA−NH_2	2749	1375.5, M + 2H	
2	sl−WALP23−C2	Ac−GC(sl)WLALALALALALALALALWWA−NH_2	2620	1311, M + 2H	
4	sl−WALP23−C4	Ac−GWWC(sl)ALALALALALALALALWWA−NH_2	2693	1347.5, M + 2H	
6	sl−WALP23−C6	Ac−GWWLAC(sl)ALALALALALALALWWA−NH_2	2693	1347.5, M + 2H	
8	sl−WALP23−C8	Ac−GWWLALAC(sl)ALALALALALALWWA−NH_2	2693	1347.5, M + 2H	
10	sl−WALP23−C10	Ac−GWWLALALAC(sl)ALALALALALWWA−NH_2	2693	1347.5, M + 2H	
12	sl−WALP23−C12	Ac−GWWLALALALAC(sl)ALALALALWWA−NH_2	2693	1347.5, M + 2H	
14	sl−WALP23−C14	Ac−GWWLALALALALAC(sl)ALALALWWA−NH_2	2693	1347.5, M + 2H	
16	sl−WALP23−C16	Ac−GWWLALALALALALAC(sl)ALALWWA−NH_2	2693	1347.5, M + 2H	
18	sl−WALP23−C18	Ac−GWWLALALALALALALAC(sl)ALWWA−NH_2	2693	1347.5, M + 2H	
20	sl−WALP23−C20	Ac−GWWLALALALALALALALAC(sl)WWA−NH_2	2693	1347.5, M + 2H	
22	sl−WALP23−C22	Ac−GWWLALALALALALALALALWC(sl)A−NH_2	2620	1311, M + 2H	2621, M + H
23	sl−WALP23−C23	Ac−GWWLALALALALALALALALWWC(sl)−NH_2	2735	1368.5, M + 2H	
24	sl−WALP23−C	Ac−GWWLALALALALALALALALWWAC(sl)−NH_2	2806		2807, M + H
26	sl−WALP23−AAC	Ac−GWWLALALALALALALALALWWAAAC(sl)−NH_2	2948		2949, M + H

[a] Ac is an N-terminal acetyl group; $-NH_2$ is a C-terminal amide ($-CONH_2$), and C(sl) is a nitroxide-labeled cysteine residue. [b] Electrospray ionization. [c] MALDI.

added (from a stock solution in trifluoroethanol) methanethiosulfonate (2 equiv, Toronto Research Chemicals). The mixture was stirred for 3 h at room temperature.

Spin-labeled peptides were purified by HPLC on a C4 or C8 reverse-phase column (Vydac 214TP54 or 208TP52) or on a Kromasil Cyano column (Western Analytical Products Inc., Cat. no. KR60-5CN-150A). For all peptides except WALP23-C22, CAA-WALP23, and WALP23-AAC, the C8 column was used with the solvent gradient 80−100% methanol with 0.1% trifluoroacetic acid over 40 min and a flow rate of 0.28 mL/min. The retention times of the peptides are ∼30 min. The spin-labeled peptides, WALP23-C22, CAA-WALP23, and WALP23-AAC, required more extensive purification. For spin-labeled WALP23-C22, the crude peptide was first purified on the Cyano HPLC column using 20−100% acetonitrile with 0.1% trifluoroacetic acid over 60 min at a flow rate of 0.8 mL/min. The peptide eluted at ∼50 min and was further purified on the C4 HPLC column using 90−95% acetonitrile with 0.1% trifluoroacetic acid over 10 min and then 95−100% acetonitrile with 0.1% trifluoroacetic acid over 50 min at a flow rate of 0.4 mL/min. The pure spin-labeled WALP23-C22 peptide eluted at ∼20 min. The spin-labeled peptides, CAA-WALP23, and WALP23-AAC were purified on the Cyano column as described for WALP23-C22 and then were submitted to further purification on the C4 HPLC column using 80−89.5% acetonitrile with 0.1% trifluoroacetic acid over 10 min and then 89.5−100% acetonitrile with 0.1% trifluoroacetic acid over 50 min at a flow rate of 0.4 mL/min. Both peptides eluted at ∼25 min.

All spin-labeled WALP peptides were analyzed by electrospray ionization tandem mass spectrometry on a Bruker Esquire ion trap instrument operating in positive mode and with a collision energy of 110 V. The peptides were dissolved in methanol containing 1% acetic acid prior to injection. Peptide fragment ions were analyzed with the Peptide Tools software (Hewlett-Packard). The peptides sl-CAA-WALP23, sl-C-WALP23, sl-WALP23-C22, and sl-WALP23-AAC did not ionize well by electrospray ionization and were therefore analyzed by MALDI using a Bruker Biflex III Time-of-Flight spectrometer. A 10 μM solution of peptide in methanol/0.1% trifluoroacetic acid was spotted onto the MALDI plate along with the matrix (10 mM α-cyano-4-hydroxycinnamic acid in 50% ethanol/50% 0.1% trifluoroacetic acid). The reflecting voltage was 1800 V, and the ion mode was positive. Mass spectrometry data are given in Table 1.

CD Spectroscopy of Peptides. Spin-labeled WALP peptides were analyzed by CD spectroscopy after embedding them in phospholipid vesicles. HPLC-purified peptides were dissolved in chloroform/methanol (1/1, v/v), and the peptide concentration was estimated from the absorbance at 280 nm (peptide concentration 0.07 mg/mL). Stock solutions of DOPC and DOPM (Avanti Polar Lipids, Inc.) were prepared in chloroform/methanol (1/1, v/v) at 50 mg/mL. Peptide and phospholipid stock solutions were mixed to give a peptide-to-phospholipid mole ratio of 1/30. Solvent was removed in a Speed-Vac (Savant Instruments), and the dried lipid film was hydrated with 0.2 mL of EPR buffer (50 mM Tris, pH 7.4). The sample was mixed with a vortex mixer for 1 min and then submitted to 10 cycles of freezing (dry ice/ethanol), thawing (room temperature water bath), and mixing on a vortex mixer for 1 min. The sample was placed in a high-powered bath sonicator (Lab Supplies) and sonicated for 20 min in a glass tube. After sonication, the samples were centrifuged at 30 000*g* for 15 min, and the supernatant was transferred to a new tube and used to obtain CD spectra at room temperature on a Jasco J-720 spectropolarimeter using a 0.1 mm path length sample cell (1 nm bandwidth, 0.2 nm resolution, 1 s response time, 20 nm/min scan speed).

Preparation of Samples for EPR Studies. EPR samples were prepared by mixing the peptide and phospholipid stock solutions (see above) to give a peptide-to-phospholipid molar ratio of 1/100. Solvent was removed in a Speed-Vac, and the residue was rehydrated with 30 μL of EPR buffer with or without 50 mM nickel (II) ethylenediamine-*N*,*N*′-diacetic acid (NiEDDA). The concentration of phospholipid in the EPR sample was typically 10 mM. The suspension was mixed on a vortex mixer for 1 min and submitted to 10 freeze−thaw cycles to make multilamellar vesicles (MLV). Vesicle size was characterized with a BIC Particle Analyzer (Brookhaven Instruments) and found to be 0.130 microns with a polydispersity of 0.237.

Time Domain and Continuous Wave EPR Spectroscopy. Pulsed saturation recovery (pSR) and pulsed electron−electron double resonance spectra were acquired on a time domain EPR spectrometer that is equipped with a loop-gap resonator (LGR).[21,32] The time resolution of the spectrometer is 5 ns per point. A typical pSR experiment used a 200 ns pulse with 20 dbm of microwave power. The dead time was 90 ns, and the microwave power during the observer period was −12 dbm. Each pSR spectrum consisted of 4.8×10^6 scans (half of which were on resonance and half were off resonance, for background control). At least two repeats of 1024, 2048, and 4096 point spectra were obtained for each experimental condition (the acquisition time for 4096 points is ∼40 min). All pSR measurements were acquired with the pump and observed microwave frequencies located on the central ^{14}N manifold of the nitroxide. Continuous wave spectra were acquired on the time domain instrument with resolution of 1024 over 90 G and also on a Bruker X-band EMX spectrometer with 1024 points over 160 G (typically for 30 min). The modulation amplitude was 1 G, and the modulation frequency was 10 kHz. All samples used in the LGR consisted of 5 μL of sample placed in a gas permeable 0.8 mm i.d.

(32) Hyde, J. S.; Froncisz, W. *J. Magn. Reson.* **1982**, *47*, 515−521.

Teflon capillary tube (Zeus industries) and were exposed to either a continuous stream of N_2 gas or medical air (21% O_2) at 21 °C during acquisition.

Each pSR spectrum was fit to a single exponential and also to a sum of two exponentials using a Marquardt−Levenberg algorithm in a global analysis environment[33] to extract the spin−lattice relaxation rate (R_1). The fitting to two different models aided in determining the effect of early time data. Oxygen and NiEDDA are both paramagnetic relaxants and will enhance the spin−lattice relaxation rate of the nitroxide spin label by collisional interaction. The spin−lattice relaxation rate was measured with and without either oxygen or NiEDDA. The contribution to the relaxation rate is proportional to the local concentration of the relaxant that is colliding with the spin label.

$$R_1^{\text{relaxant}} = R_1^{\text{no relaxant}} + \chi[\text{relaxant}] \tag{1}$$

The proportionality constant called the relaxivity, χ, is, in turn, proportional to the relative translational diffusion rate of the relaxant and spin label, D, which is the sum of the translational diffusion rates of the spin label and the relaxant [D(SL) + D(relaxant)]. χ also depends on the efficiency of a given collision to produce relaxation of the nitroxide spin, p, and the interaction distance, r.[6]

$$\chi = 4\pi rp(D(\text{SL}) + D(\text{relaxant})) \tag{2}$$

The two experimental measurements of R_1^{relaxant} and $R_1^{\text{no relaxant}}$ are used to calculate χ[relaxant] from the difference in relaxation rates:

$$\Delta R_1 = R_1^{\text{relaxant}} - R_1^{\text{no relaxant}} = \chi[\text{relaxant}] \tag{3}$$

ΔR_1 values for oxygen and NiEDDA are the time domain analogues of the Hubbell Π parameter.[11,21,31] The ratio $\Delta R_1^{O_2}/\Delta R_1^{\text{NiEDDA}}$ is useful because $\chi_{O_2}/\chi_{\text{NiEDDA}}$ has been assumed by others to be approximately a constant throughout in the lipid environment.[11,31] Consequently

$$\Delta R_1^{O_2}/\Delta R_1^{\text{NiEDDA}} \mu\propto [O_2]/[\text{NiEDDA}] \tag{4}$$

The ratio of concentrations (eq 4) can be interpreted in terms of a relative chemical potential of O_2 and NiEDDA. The time domain analogue of the Hubbell Φ parameter[11,31] is

$$\Phi = \ln(\Delta R_1^{O_2}/\Delta R_1^{\text{NiEDDA}}) \tag{5}$$

The logarithm is taken so that Φ is directly proportional to the difference in chemical potential of O_2 and NiEDDA.

It is possible to infer changes in local probe motion from both the continuous wave (CW) EPR and the spin−lattice relaxation rates. The motional parameter chosen from the CW-EPR spectrum is the peak-to-trough "line width" of the center ^{14}N hyperfine line. This quantity is a monotonic function of the local dynamics. The slower the motional process, the larger the line width. The mobility parameter, defined by Hubbell and co-workers, is linearly related to the inverse of the line width.[24] The spin−lattice relaxation rate is also a monotonic function of the mobility. The slower the mobility, the smaller the spin−lattice relaxation rate.[25] Both of these parameters are used to estimate the probe's mobility as a function of the placement in the bilayer.

Data Modeling. To obtain a relation between peptide residue number and the distance along the axis of the peptide, an idealized regular α-helix consisting of 23 alanine residues was modeled. The alanine peptide coordinates were obtained from the Insight II software package (MSI/Accelrys). The purpose of this helix is to provide a scale that indicates the distance between residues (hence spin probes) and the approximate placement of a given spin probe in the bilayer. The α-carbons of the peptide backbone best fit a helix with a rise of 1.537 Å per residue. To obtain a distance scale within the membrane bilayer, the helix was superposed on the density profile of the phospholipid components of a DOPC bilayer, determined by X-ray scattering and Neutron diffraction.[34,35] We let x denote the distance from the center of the bilayer. The center of the helix is taken to be at residue 12 because this is the average of the two tryptophans at residues 2 and 22, which register the WALP peptide with the bilayer. The position is related to the residue number of WALP23, rn, by the rise of the helix.

$$x = 1.537(rn - 12) \tag{6}$$

This formula includes all residue numbers, even those where the original WALP23 is extended (see Table 1). The full range of residue numbers is from −2 to 26. The offset of the WALP peptide from the center of the bilayer is denoted by $\bar{x}$.

We model the relaxation data set by a continuous, symmetric, smooth function. The modeling by a smooth function converts the data, obtained at discrete positions in the membrane, into a continuous function expressed in terms of a few parameters, such as the distribution's mean position and width. Such modeling allows the comparison of different data sets by directly comparing the parameters of the model. The function chosen to model the relaxation rates is

$$S(x;\bar{x},l,a) = \frac{1}{4l}\left\{\tanh\left(\frac{x-\bar{x}+l}{a}\right) - \tanh\left(\frac{x-\bar{x}-l}{a}\right)\right\} \tag{7}$$

The function S is an even, symmetric function about the center value, $\bar{x}$, and has unit area. The function goes to zero as $|x|$ becomes large. The function makes a transition at $\pm l$, and the width of the transition is given by a. This function behaves much like a normalized Gaussian function, which has two adjustable parameters, $\bar{x}$ and σ, and is defined as: $G(x;\bar{x},\sigma) = 1/\sigma\sqrt{2\pi}\cdot e^{-(x-\bar{x})^2/2\sigma^2}$. When $l = 1.618a$, the above S function closely approximates a Gaussian with the standard width of the Gaussian, σ, being proportional to the transition width, $\sigma = 1.397a$. When the transition width is much less than the transition position, $a \ll l$, the S function has a "top hat" shape. The S function has one more adjustable parameter than a Gaussian and was chosen because that additional flexibility was deemed necessary to fit the relaxation rate profiles. The normalized symmetric function (eq 7) is used to model the spin−lattice relaxation rates with a scale or proportionality factor between the symmetric function and the data, as well as a baseline value that will be the amount of relaxation outside of the membrane, where the symmetric function (eq 7) is nearly zero. Therefore, the complete fitting function is

$$\hat{Y}(x) = mS(x;\bar{x},l,a) + b \tag{8}$$

Because the symmetric function (eq 7) has unit area, m is related to the integral over the distance parameter, x, and is independent of the precise form of the smooth, continuous function:

$$m = \int_{-\infty}^{\infty} [\hat{Y}(x) - b]\mathrm{d}x \tag{9}$$

All of the parameters, $\{\bar{x}, l, a, m, b\}$, are determined by a least-squares fit of the relaxation data to the model function of eq 8.

Average Oxygen Concentration and Relaxivity in the Membrane from the Relaxation Profile. The scale factor, found in eqs 8 and 9, is obtained directly in terms of the relaxation rates themselves and has meaning, independently of the model function.

$$m = \int_{-\infty}^{\infty} (\hat{Y} - b)\mathrm{d}x = \int_{-\infty}^{\infty} (\Delta R_1(x) - \Delta R_1^{\text{bulk}})\mathrm{d}x \cong \sum (\Delta R_1(x_j) - \Delta R_1^{\text{bulk}})\Delta x \tag{10}$$

Therefore, if the bulk relaxation value is known (outside the membrane), the sum or integral can be computed over the entire data set. The

(33) Mailer, C.; Robinson, B. H.; Williams, B. B.; Halpern, H. J. *Magn. Reson. Medcine* **2003**, *49*, 1175−1180.
(34) White, S. *Biophys. J.* **1991**, *59*, 162−173.
(35) White, S. H.; Wimley, W. C. *Curr. Opin. Struct. Biol.* **1994**, *4*, 79−86.

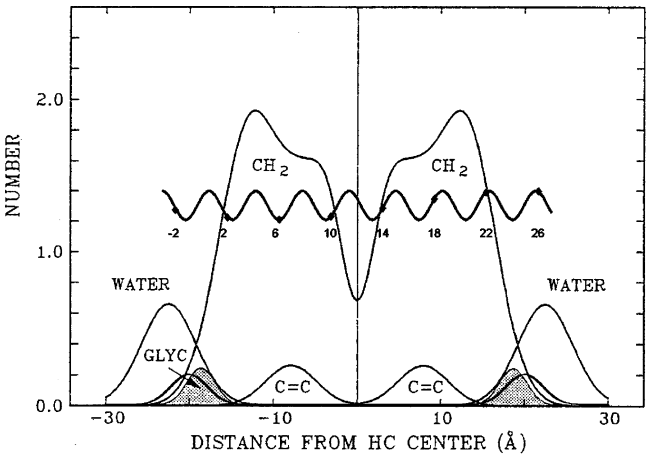

Figure 1. A comparison of a polyalanine transmembrane α-helix with the probability profiles of different molecular components of DOPC.[34] Maximum probability for the PC headgroup component coincides with the waters of hydration (this portion of the figure is courtesy of Dr. S. White, University of California, Irvine). The residue positions correspond to the position of backbone α-carbons.

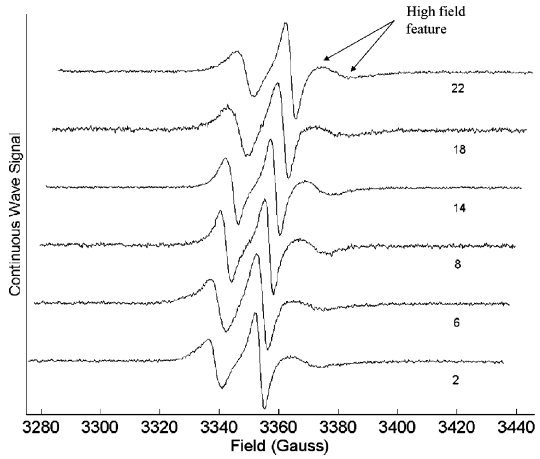

Figure 2. Set of CW spectra for positions 2, 6, 8, 14, 18, and 22 of WALP in DOPC at 21 °C. The field axis applies to the bottom spectrum; each spectrum is offset by 1.5 G to the right (relative to the one below) to avoid overlap.

distance between residues, Δx, is related to the rise per base pair. Such a sum (or integral) will converge regardless of how far the protein extends into the aqueous solvent. We can determine the average relaxation rate within the bilayer, $\langle \Delta R_1^{\text{bilayer}} \rangle$. Such a quantity is $\langle \Delta R_1^{\text{bilayer}} \rangle = \langle \Delta\Delta R_1 \rangle + \Delta R_1^{\text{bulk}}$, where the average relaxation rate over the aqueous−bulk relaxation rate is given by

$$\langle \Delta\Delta R_1 \rangle = 1/L \int_{-\infty}^{\infty} (\Delta R_1(x) - \Delta R_1^{\text{bulk}}) \mathrm{d}x \simeq m/L$$

The thickness of the bilayer, L, must be determined by an independent experiment related to the volume of the bilayer added. There is no abrupt edge to the relaxation profile that would define the bilayer thickness.

The Supporting Information provides the approximations that are necessary to allow a separation of the average bilayer relaxation rates into two separate averages, one of the oxygen diffusion rate and the other the oxygen concentration, so that $\langle \Delta R_1 \rangle = \langle \chi \cdot [O_2] \rangle \approx \langle \chi \rangle \cdot \langle [O_2] \rangle$. This separation of averages allows an approximate relation between the ratio of relaxation rates and the translational diffusion coefficient times the equilibrium constant, K, for oxygen.

$$\left(\frac{\langle \Delta R_1^{\text{bilayer}} \rangle}{\Delta R_1^{\text{bulk}}} \right) = \frac{\langle D^{\text{bilayer}} \rangle}{D^{\text{bulk}}} K$$

Results

WALP Registration in the Membrane. The secondary structure of spin-labeled WALP23 peptides in membranes was characterized by circular dichroism (CD) spectroscopy. The line shapes of the CD spectra for sl-WALP23-C12 in DOPC vesicles and sl-WALP23-C12 in DOPC vesicles both show minima near 222 and 208 nm and a maximum near 190 nm. The extremes in the CD spectra indicate that the sl-WALP23-C12 peptide has an α-helical conformation when incorporated into DOPC or DOPM vesicles. The CD spectra of the WALP23 peptides that were spin-labeled at other sites (C4, C8, C16, C20, and C23) have a similar appearance. CD spectra for C12 are given in the Supporting Information (Figure 1S).

Figure 1 shows the probability distribution of the various components in DOPC membranes as a function of distance from the center of the distribution of the hydrocarbon residues (i.e., the bilayer) as determined by a combination of neutron scattering and X-ray crystallography.[34,35] A model α-helix (see Materials and Methods) is superimposed with the density profiles to illustrate the probable co-registration of the WALP23 protein with the bilayer. The helical coil passes through all α-carbon atoms in the polypeptide. The residues are numbered as in Table 1. The fitting was done so that the two outer tryptophans of WALP23 (residues 2 and 22; see Table 1) are equidistant from the center of the bilayer. As a result, residues 2 and 22 are coincident with the maximal density of the carbonyl residues of the DOPC. This registration indicates that the length of the WALP23 protein is very close to the DOPC membrane thickness, and therefore, one would anticipate very little readjustment of the membrane thickness either in the vicinity of the WALP23 or in the helical parameters of the WALP23 itself.[15,36] The WALP23 peptide was extended by adding alanine residues after the tryptophans on the C-terminus and before the tryptophans of the N-terminus (see Table 1). Examination of Figure 1 shows that the residues of the extended WALP peptides (−2 and 26, Table 1) do not protrude past the choline headgroup region or the interfacial water and do not reach the bulk aqueous region beyond the interfacial aqueous region.

Continuous Wave EPR and Spin-Label Motion in the Membrane. The low-power continuous wave first harmonic absorption EPR spectrum of each of the spin-labeled peptides (see Table 1) was obtained for WALP incorporated into DOPC and DOPM membranes. Figure 2 displays a set of CW spectra for those WALP proteins spin labeled at positions 2, 6, 8, 14, 18, and 22 in DOPC at 21 °C. CW spectra for the same labeling positions of WALP in DOPM are shown in Figure 2S of the Supporting Information. The CW spectra are all very similar in appearance, indicating that the local conformational freedom of the spin label is similar throughout the bilayer and is independent of the lipid composition (PC or PM). Careful inspection of the high-field feature (see arrow on Figure 2) of the CW spectra in Figure 2 shows that the high-field features of positions 8 and 14 are slightly sharper than those of the others. Generally, spectra with sharper features are indicative of more rapid motion of the spin probe. As nitroxide spin-label motion

(36) Demmers, J. A. A.; vanDuijn, E.; Haverkamp, J.; Greathouse, D. V.; Koeppe, R. E., II; Heck, A. J. R.; Killian, J. A. *J. Biol. Chem.* **2001**, *276*, 34501−34508.

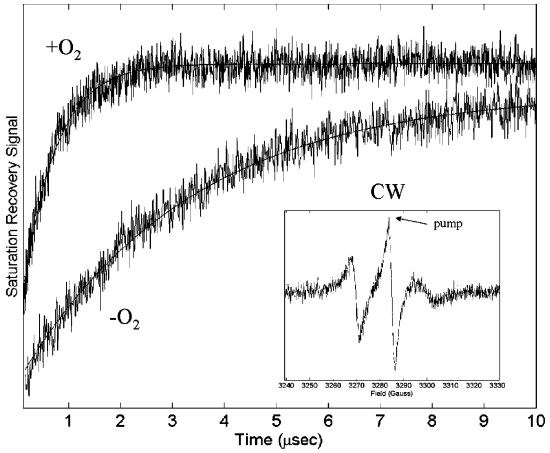

Figure 3. First 10 μs of a typical pSR spectrum with and without oxygen (see Materials and Methods). Solid lines are single-exponential fits to the pSR spectrum. The insert is the low-power CW spectrum. The arrow shows placement of the pump pulse and observed field for pSR.

slows, the high-field feature flattens.[21] The trend observed in Figure 2 indicates that the spin label has slightly more conformational freedom in the center of the bilayer. Another measure of spin-label dynamics is the peak-to-peak line width, ΔH_{pp}, of the central EPR feature. ΔH_{pp} monotonically increases as the motion of the nitroxide decreases within the regime of dynamics encountered here. The inverse of ΔH_{pp} is linearly related to the "mobility parameter" of Hubbell and co-workers.[24] ΔH_{pp} is plotted as a function of the residue number of the spin-label position on WALP in the membrane bilayer for DOPC in Figure 4 and DOPM in Figure 5 (as open squares). Tables 1S and 2S of the Supporting Information give the measured ΔH_{pp} for all peptide-labeling positions for WALP peptide in DOPC and DOPM.

Time Domain EPR Measurements of O_2 and NiEDDA Relaxation Profiles in DOPC and DOPM. Figure 3 shows the first 10 μs of a typical pSR signal with and without oxygen for WALP23 spin labeled at position 2 in DOPM vesicles. The smooth solid lines are single-exponential fits to the pSR spectrum. The values of the nitroxide spin−lattice relaxation rates in the presence and absence of spin relaxants are shown in Figures 4 and 5 (filled diamonds) as a function of the labeling position (data are given in Tables 1S and 2S, Supporting Information). Further analysis of the spectra, assuming a biexponential function, was carried out. The result is that the second exponential is not significant. The pSR signals are accumulated when the magnetic field is set to the center resonance position of the CW spectrum, shown as an insert in Figure 3.

The $\Delta R_1(O_2)$ values (see eq 3) are shown in Figures 4 and 5 (filled squares) for the WALP protein in DOPC and DOPM, respectively. The solid line that fits the $\Delta R_1(O_2)$ data in Figures 4 and 5 is the best fit of the symmetric profile function $\hat{Y}(x)$ (eq 8) to the data. The least-squares optimized values of $\bar{x}$, l, a, m, and b (see Materials and Methods) are given in Table 3S of the Supporting Information.

If the WALP peptide were perfectly centered in the bilayer, the offset parameter would be $\bar{x} = 0$ Å. This offset value neglects the difference in distance between the nitroxide and the backbone α-carbon to which it is attached. The mean position for the center of the peptide for the DOPC membrane (Figure 4), determined from the least-squares fit to the ΔR_1 data, is $\bar{x} = -0.5 \pm 0.2$ Å, which is very close to the ideal center. The transition region of the fitting function, which is $2l$ (see Materials and Methods), is ~10 Å wide, and the transition width is large enough so that the curve changes smoothly with residue number. For the DOPC membrane, $l/a \approx 1.21$. Therefore, the shape of the fitting function is not far from a Gaussian with a half-width of ~5.4 Å. The fitting coefficient, m, was determined by the least-squares fit of the model function to the data. However, m may also be computed directly by the summation in eq 10. The direct summation of the relaxation rates, in which $\Delta x = 2 \times 1.537$ Å, gives the same value as that obtained by the symmetric model function.

The ΔR_1 values for the relaxant NiEDDA are shown in Figure 4 (solid circles). The solid line through these data is the fit to the symmetric function (eq 8) (see Table 3S of the Supporting Information for best-fit parameters). It was not possible to measure the effects of NiEDDA around the center of the bilayer at the concentration of relaxant used because NiEDDA does not partition well into the hydrophobic core. The analytic concentration of NiEDDA is 50 mM. The effect of the NiEDDA relaxant near the headgroup region should be compared with the effect of NiEDDA on surface-labeled aqueous proteins.[37,38] When the spin label is on the surface of a water-soluble protein, NiEDDA induces an increase in the relaxation rate of around 3 Mrad/s at a 10 mM bulk concentration. The NiEDDA relaxation on the most exposed residue in the present study is about 25 times less effective than that expected from previous studies using NiEDDA on surface-exposed residues of water-soluble proteins. An examination of Figure 1 underscores the observation that the NiEDDA relaxant never encounters spin-labeled residues fully in the bulk aqueous environment.

The CW line width and spin−lattice relaxation rates in the absence of oxygen or NiEDDA, shown in Figures 4 and 5, contain information on spin-label dynamics. The solid lines that fit the spin−lattice relaxation rates, R_{1e}^{o}, in Figures 4 and 5 were generated assuming that the data are described by the sum of two symmetric functions (eq 7). One of the symmetric components of the profile was constrained by using the l and a values from the fit to the $\Delta R_1(O_2)$ data. The second symmetric component assumes that there is a reduction in relaxation at the interfacial region of the bilayer, represented by a negative scaling m. The equation used (for Figures 4 and 5 for the two different bilayers) is

$$\hat{R}_{1e}^{Fit} = m_1 \times S(x;\bar{x}_1,l_1,a_1) + m_2 \times S(x;\bar{x}_2,l_2,a_2) + b \quad (11)$$

The values of the fitting parameters are given in Table 3S of the Supporting Information. The R_{1e}^{Fit} curves were used to demonstrate that the line widths, ΔH_{pp}^{*}, followed similar trends. The R_{1e}^{Fit} curves were superposed on the ΔH_{pp}^{*} data with a translation and offset for both DOPC and DOPM [Figures 4 and 5, as solid lines through ΔH_{pp}^{*} data (open squares)]. No attempt was made to optimize the fit to the ΔH_{pp}^{*} values.

Figure 6 shows the log of the ratio of the relaxation rates for the two relaxants, oxygen and NiEDDA, in DOPC vesicles, plotted as open squares (see eq 5, Materials and Methods). The

(37) Ball, A.; Nielsen, R.; Gelb, M. H.; Robinson, B. H. *Proc. Natl. Acad. Sci. U.S.A.* **1999**, *96*, 6637−6642.
(38) Lin, Y.; Nielsen, R.; Murray, D.; Hubbell, W. L.; Mailer, C.; Robinson, B. H.; Gelb, M. H. *Science* **1998**, *279*, 1925−1929.

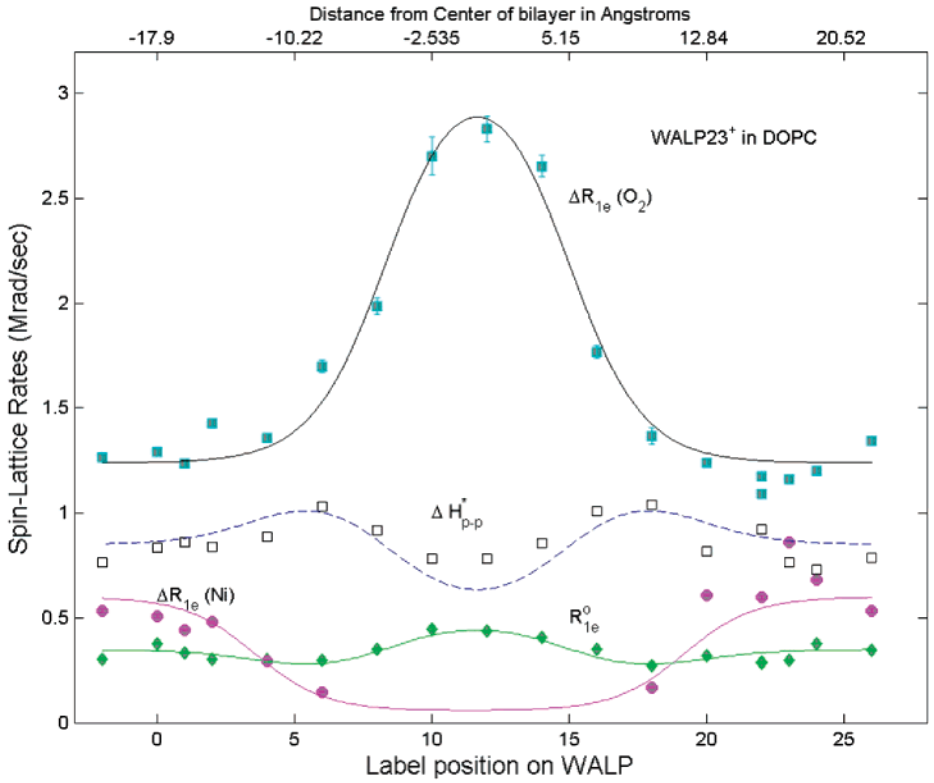

Figure 4. Relaxation rate data for spin-labeled WALP (and extended WALP, Table 1) in DOPC at 21 °C. The nitroxide spin−lattice relaxation rates, R^{o}_{1e}, without any spin relaxant are shown as solid diamonds. The center line width, ΔH_{pp} is converted to frequency units and scaled to be similar in magnitude to the spin−lattice relaxation rate, $\Delta H^{*}_{pp} = \gamma_e/75\ (2/\sqrt{3})\ \Delta H_{pp}$ (open squares). The ΔR_1 relaxation rates are for O_2 (solid squares) and NiEDDA at 50 mM (solid circles). The solid line fit to the data uses the least-squares optimized values discussed in the text. The axis across the top is the distance from the center of the membrane bilayer (see Figure 1) in angstroms assuming that the α-carbon of residue 12 is centered in the bilayer: $x = 1.537 \times rn - 18.44$. The two data points at position 22 correspond to the two entries in Table 1S of the Supporting Information.

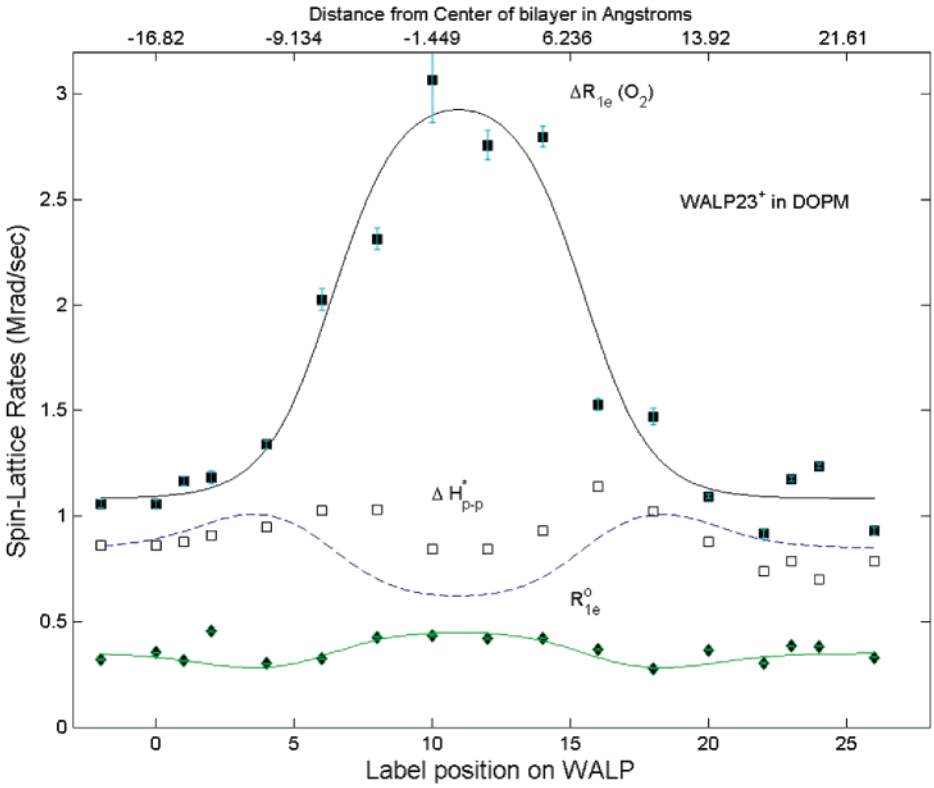

Figure 5. Relaxation rate data for spin-labeled WALP (and extended WALP, Table 1) in DOPM at 21 °C. See legend of Figure 4.

smooth, solid line is the ratio of the fitting functions from the fits to the two data sets in Figure 4. The linear triangle fit, which peaks at residue 12, is the linear model of the Φ parameter suggested by Altenbach et al.[12] The Φ profile must achieve a

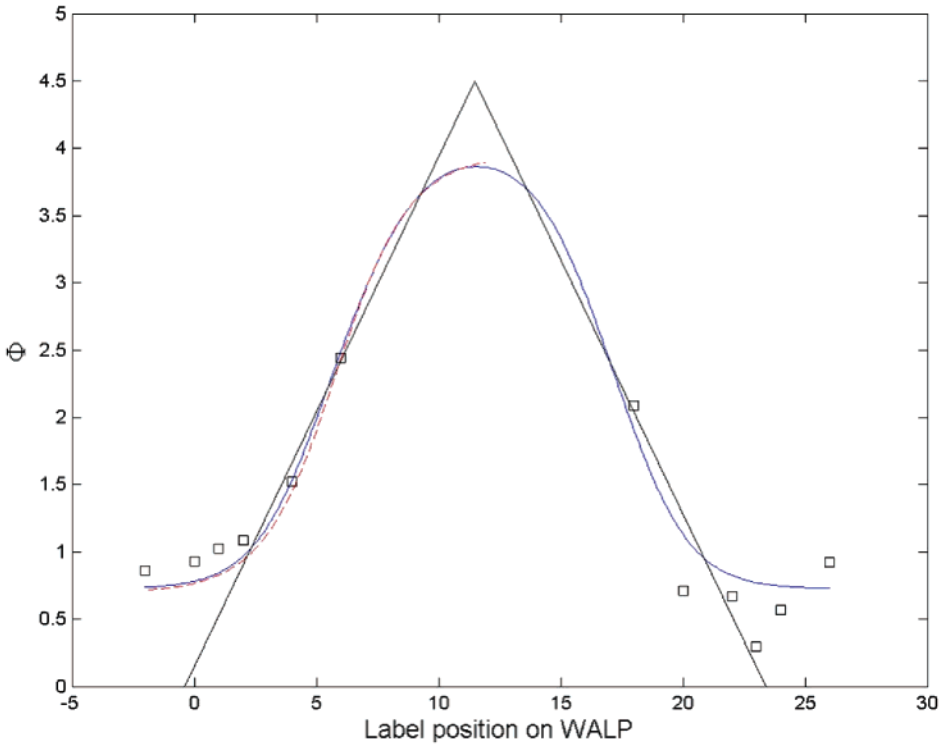

Figure 6. The Φ parameter, adapted from Altenbach et al.,[12] (see eq 5, text) plotted for WALP in DOPC; (open squares) ratio of O_2 and NiEDDA data (see Figure 4); (solid lines) ratio of O_2 and NiEDDA fitting functions (see Figure 4). Straight lines are the linear approximation of Altenbach et al.;[12] (dashed lines) the one-sided model of Φ adapted from Frazier et al.[31] ($\Phi = 13/8 \tanh(rn - 5.8/3) + 19/8$).

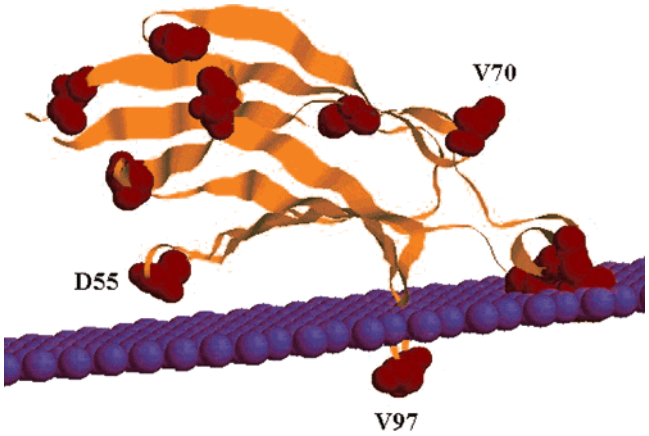

Figure 7. C2 domain of cytosolic phospholipase A_2. Orientation of the domain was determined by the EPR technique in Ball et al.[37] The plane represented by the purple balls consists of the phosphate region of the phospholipid bilayer. Red balls are spin-labeling sites. Relaxation data for sites V97 and V70 are given in Table 3.

plateau as the environment traverses to aqueous bulk conditions. The dashed line is of the functional form suggested by Frazier et al.,[31] which incorporates a smooth transition of Φ to its aqueous value.

Discussion

Peptide Dynamics. It is remarkable that the basic spin−lattice relaxation rates, in the absence of any relaxants, are almost independent of peptide-labeling position when WALP is incorporated in the bilayer. The uniformity of the CW EPR spectra is consistent with the trends seen by the time-domain-measured spin−lattice relaxation rates. The general effect of dynamics on R_{1e}^{o} is that faster nitroxide motion will increase the value of R_{1e}^{o}. In contrast, the CW line width, ΔH_{pp}, will increase with slower motion and eventually become an ambiguous measure of dynamics.[21] The CW "mobility parameter" that is sometimes used to gauge dynamics[24] is based on the reciprocal of the line widths. Plots of R_{1e}^{o} and ΔH_{pp} are shown in Figures 4 and 5. Experimental calibrations that relate the correlation time of isotropic spin-label motion to the value of the spin−lattice relaxation rate have been developed.[21,25,39] While the spin label on WALP is in an anisotropic environment, the isotropic calibration can be used as a rough estimate of correlation time. Both time domain and CW measurements indicate that there is a slight decrease in spin-label mobility near the lipid−water interface (less than a factor of 2 in the assigned correlation time) and a slight increase in mobility in the central region of the bilayer. The solid lines, overlaid on R_{1e}^{o} and ΔH_{pp}^{*}, are only shown to give the general trends and are not based on any first principles model. The results are similar for both DOPC and DOPM membranes. The relative insensitivity of the WALP relaxation rates on labeling position is in stark contrast to the trends observed when using spin-labeled lipids or lipid analogues, such as spin-labeled *n*-doxyl stearic acid. Spin-labeled *n*-doxyl stearic acid relaxation rates indicate a large increase in mobility of the spin label as the labeling site moves toward the center of the bilayer (more than an order of magnitude in the correlation time of motion as the labeling site moves from the 5 to the 16 position of spin-labeled *n*-doxyl stearic acid[40]). The contrast of our data with spin-labeled *n*-doxyl stearic acid data is even more remarkable when it is realized that the effective viscosity of the bilayer for a transmembrane protein is highly anisotropic and orders of magnitude larger in the bilayer than

(39) Percival, P. W.; Hyde, J. S. *J. Magn. Reson.* **1976**, *23*, 249−257.
(40) Mailer, C.; Nielsen, R. D.; Robinson, B. H. *J. Phys. Chem.* In press.

in the aqueous phase.[41,42] The diffusion coefficient for small molecules, such as water, can be an order of magnitude smaller in the bilayer than in bulk water.[28] The spin probe resides at a lipid−protein interface. Any contribution to the probe's dynamics from the protein will be independent of the depth in the membrane. A mechanism by which the protein plays an important role in the probe's dynamics has been suggested: conformational freedom of the probe is restricted by bonding of a sulfur from the MTSSL spin-label linkage to the C_α hydrogen of the peptide backbone.[24] Therefore, the lipid environment only partially contributes to the probe's dynamics. The extent of that contribution is unknown and may be minimal. In future work, it may prove interesting to craft a spin probe attached to the same polypeptide by a longer tether to more extensively probe the lipid contribution to the dynamics at this interface.

The local protein sequence can potentially affect the spin-label dynamics and relaxivity of oxygen. The majority of the WALP residues that were labeled are flanked on either side by two alanines. The local environment at these labeling sites should not shield the spin label from intermolecular interaction with either the lipids or oxygen because the MTSSL linkage extends the spin label beyond where the alanine side chain can reach. In two cases, however, where the cysteine is placed in positions 2 and 22, the cysteine is flanked by a G and a W, and a W and an A, respectively. In both cases (positions 2 and 22), nothing remarkable was observed; the spin−lattice relaxation rates themselves and the change in relaxation due to the relaxants in both membranes for these two residues were in line with those nearby. Moreover, the CW signals (and ΔH_{pp} values) indicate no anomalies in positions 2 and 22 relative to the rest of the labeling positions.

In summary, the motion of the peptide-bound nitroxide in the membrane is very similar to that seen in nitroxides similarly attached to α-helices on the surface of water-soluble proteins that are interpreted as being at solvent-exposed surfaces.[43,44] The spin label shows similar dynamics and similar ordering whether in aqueous phase or in membranes. This is in contrast to what has been observed for the dynamics determined from studies of spin-labeled lipids in membranes.

Modeling the Insertion of WALP in Membranes. Given that the helical rise of an α-helix is 1.5 Å per residue (see Materials and Methods), the calculated length of the WALP23 leucinyl−alanyl repeat is approximately 26 Å, which is very close to the hydrophobic thickness of the DOPC bilayer (27 Å).[45] As indicated by Killian, membrane proteins which have one or more hydrophobic α-helical segments spanning the lipid may cause local disruption of lipid order or may preferentially recruit the best-matching lipids when the membrane is composed of different lipids.[46] The peptide configuration may also be disrupted as a result of incorporation in the bilayer.[46] The WALP peptide is matched with the DOPC lipid[15] and so avoids various mismatch tendencies, such as helix tilting, aggregation, and backbone adaptation. The CD spectra of the sl-WALP peptide in DOPC confirm the α-helix conformation. Figure 1 further indicates the best fit between the membrane and WALP peptide based on symmetry arguments.

The offset of the center of the ΔR_1 profile is different between DOPC and DOPM bilayers. A comparison of the abscissa offset, $\bar{x}$, of the fitting function $\hat{Y}$ between Figures 4 and 5 shows a small but measurable difference. The profile offset suggests about a 1 Å (-1.1 ± 0.4 Å; see Table 3S of the Supporting Information) difference in the center of the WALP peptide when comparing the two membrane bilayers. The registration shown in Figure 1 is, therefore, moved to the right for WALP in DOPM. This shift can be understood in terms of the electrostatics of the peptide; DOPC is a neutral (zwitterionic) membrane, and it is expected that the relaxant profile should be centered about the membrane. The observed offset of 0.5 ± 0.2 Å in DOPC is consistent with this hypothesis. The end caps of the WALP (an N-terminal acetyl group, left side, and a C-terminal amide, right side of Figure 1) produce dipoles that point from the electron-deficient N to the electron-rich O, so the dipole points toward the N-terminal group (left in Figure 1). The interaction energy between the peptide dipoles and the bilayer charge on the membrane will be lower if the protein shifts to the right from ideal registration in anionic membranes. This reduces the center mean value, which is observed experimentally. It is difficult to quantitatively estimate the energy associated with such a shift. The forces that oppose electrostatics are the registration forces due primarily to the two tryptophans at the interface. Therefore, the shift of the WALPs center is qualitatively consistent with the dipolar forces.

The symmetric functions that fit the $\Delta R_1(O_2)$ data allow extrapolation to the value of $\Delta R_1(O_2)$ in aqueous bulk. The extrapolated values of $\Delta R_1(O_2)$ from these fits are very close to the bulk value of 1.2 Mrad/s for the oxygen relaxation rate measured in other protein systems.[21] The transition to the bulk value of relaxation is another feature of the relaxation profile that aids in registration of the peptide. If the $\Delta R_1(O_2)$, due to NiEDDA, is extrapolated in a like manner, the extrapolated value for NiEDDA underestimates the value that is expected based on relaxant measurements of water-soluble proteins by a factor of 25 (see Materials and Methods). The extrapolated values of O_2 and NiEDDA are in contrast to each other. This observation suggests that the oxygen can diffuse around and through the membrane, whereas NiEDDA, about 3 times the diameter of oxygen, is significantly inhibited in its translation near the membrane. The NiEDDA reduction is perhaps due, in part, to noncovalent interactions between the NiEDDA and the membrane.

Average Values of Oxygen Diffusion and Concentration in the Bilayer from Relaxation Profiles. The relative oxygen relaxation rate, $\Delta R_1^{bilayer}/\Delta R_1^{bulk}$, is related to the relative mobility, $\chi^{bilayer}/\chi^{bulk}$, and to the equilibrium partition coefficient for oxygen, $K \equiv \langle[O_2]^{bilayer}\rangle/[O_2]^{bulk}$, where bulk values are for the aqueous phase sufficiently outside the membrane (see Materials and Methods). It is known that oxygen preferentially partitions into the membrane bilayer, so that the equilibrium constant, K, relating oxygen concentration in the bilayer relative to bulk is greater than unity, and in model systems that mimic the membrane−aqueous phases, the oxygen partition coefficient is on the order of 5−10.[4,10] We take for heuristic purposes, a

(41) Andre, J. C.; Bouchy, M.; Donner, M. *Biorheology* **1987**, *24*, 237−272.
(42) Edidin, M. *Annu. Rev. Biophys. Bioeng.* **1974**, *3*, 179−201.
(43) Lietzow, M. A.; Hubbell, W. L. *Biochemistry* **2004**, *43*, 3137−3151.
(44) Barnes, J. P.; Liang, Z.; Mchaorab, H. S.; Freed, J. H.; Hubbell, W. L. *Biophys. J.* **1999**, *76*, 3296−3306.
(45) Silvius, J. R. *Thermotropic Phase Transitions of Pure Lipids in Model Membranes and Their Modifications by Membrane Proteins*; John Wiley and Sons: New York, 1982.
(46) Killian, J. A. *FEBS Lett.* **2003**, *555*, 134−138.

representative point, near the center of the bilayer, where the concentration of oxygen is largest; For this single point, $[O_2]^*/[O_2]^{bulk} > K$, from the relaxation rate expressions (eq 3):

$$\frac{\chi^{bulk}}{\chi^*} = \frac{[O_2]^*}{[O_2]^{bulk}} \times \frac{\Delta R_1^{bulk}}{\Delta R^*_1} > K \times \frac{\Delta R_1^{bulk}}{\Delta R^{**}_1} \sim 2 \qquad (12)$$

In the data reported here, $\Delta R_1^{bilayer}/\Delta R_1^{bulk} < 3$, and the lower limit of the equilibrium constant, $K \sim 6$, was assumed. On the basis of these values, the relaxivity in the lipid bilayer is reduced by about one-half from the bulk value. This gives the general idea that the diffusion of oxygen in the membrane must be slower than that in the aqueous phase. Naively, the relaxivity, χ, of oxygen might be reduced within the membrane relative to the bulk χ in aqueous solvent because the lipid bilayer presents a sterically constrained environment where spin label and oxygen diffusion are reduced. The predictions of molecular dynamics simulations of small molecule diffusion in lipid bilayers are conflicting. One study[27] suggests just the opposite, finding that the diffusion rate (or diffusion coefficient) for oxygen (in DPPC) is about 1.5-fold larger in the bilayer than that in water, which is qualitatively in the opposite direction from the present estimate. The rationalization of this molecular dynamics result is that there are greater solvent-free voids in the lipid environment. The same study also found that the diffusion rate of water is about 4-fold larger in the bilayer than that in the bulk. The water result is important because a more recent theoretical study of water in the same bilayer [28] found that the diffusion coefficient for water is about 4-fold smaller in the bilayer than that in bulk. This more recent study casts doubt on the previous study of oxygen diffusion coefficient in the bilayer and suggests that our analysis of the partitioning of the measured relaxivity between oxygen diffusion coefficient and concentration is reasonable.

Equation 12 only uses a single point inside the bilayer. An upper bound for χ in the membrane is obtained by using averages over the entire bilayer (see Materials and Methods, and Supporting Information). Estimates of K, L, ΔR_1^{bulk}, and m are required. From the best-fit parameters for the curves in Figures 4 and 5 (see Table 3S of the Supporting Information), and assuming that $\infty > L > 10$ Å, the factor $(m/\Delta R_1^{bulk} L + 1) = (\langle \Delta\Delta R_1 \rangle / \Delta R_1^{bulk} + 1)$ in eq S3 is bounded by $1 < (m/\Delta R_1^{bulk} L + 1) < 3$; K is on the order of 5−10. This implies that $2 < (\chi^{bulk}/\chi^{bilayer}) < 10$. The most important part of this result is that the mean relaxivity in the bilayer is smaller than that in the bulk. Therefore, the diffusion coefficient for the oxygen in the bilayer is smaller (i.e., oxygen moves more slowly in the bilayer) than that in the aqueous phase. The mean diffusion rate is slowed by a factor between 2 and 10. Because the oxygen-induced relaxation rates are approximately 3 times larger in the bilayer than in the aqueous phase, the oxygen concentration must be between 6 and 30 times larger to compensate for the slower diffusion. As an example, if $K = 8$ and $L = 20$ Å, $\langle \chi^{bilayer} \rangle = \chi^{bulk}/4$ or $\langle D^{bilayer} \rangle = D^{bulk}/4$. The diffusion coefficient, D, is the relative translational diffusion coefficient, which includes the motion of the spin probe itself. The majority of the motion comes from the smaller object, the oxygen. Therefore, $\langle D_{O_2}{}^{bilayer} \rangle \approx D_{O_2}{}^{bulk}/4$. While χ and $[O_2]$ cannot be separated in the individual measurements, the average $\langle \chi^{bilayer} \rangle$ can be estimated knowing the equilibrium partition coefficient. In summary, the experimentally determined oxygen relaxation gradient provides a constraint on the diffusion coefficient and the equilibrium concentration of oxygen both as a function of position in the membrane and in terms of bulk properties. The present estimate on the relative mean diffusion coefficient discriminates between two theoretical predictions from molecular dynamics simulations.

Table 2. Oxygen-Induced Relaxation Rates Measured on Different Bilayers using Either 12-WALP or 16-slPC (All Data Obtained at 21 °C)

spin probe	bilayer	$\Delta R_1^{O_2}$ (Mrad/s)
12−WALP	DOPC	2.8
12−WALP	DOPM	2.7
12−WALP	DMPC	2.0
12−WALP	DOPS	2.0
16−slPC	POPC	2.5[a]

[a] Without any protein present; 2.5 Mrad/s with $(LL)_{12}$ present; 1.4 Mrad/s with 10 mol % $(LA)_{12}$ present.[9,48]

Comparison with Previous EPR Measurements of Oxygen Profiles. A number of studies,[5−9,13] following the seminal work of Plachy,[10] have measured oxygen relaxation parameters using spin-labeled *n*-doxyl stearic acid or spin-labeled lipids, such as spin-labeled phosphatidylcholine, in a variety of membranes. The original work of Windrem and Plachy[10] used the line width broadening, and Popp and Hyde[47] used the continuous wave progressive saturation technique. These studies demonstrated that the diffusion−solubility profile of oxygen increased in the bilayer. They used spin-labeled *n*-doxyl stearic acid with the probe at different positions along the doxyl stearic acid in various membranes, including DPPC and DSPC to obtain the profile. Subczynski et al.[6,48] used pSR and obtained quite similar diffusion−solubility profiles with spin-labeled phosphatidylcholine in POPC. In addition, they compared the oxygen profile in pure POPC and POPC with 10 mol % $(LL)_{12}$ and $(LA)_{12}$ polypeptides, again using the spin-labeled lipids as the reporter for oxygen. The peptides used by Subczynski et al. are very similar to WALP; however, the hydrophilic terminating residues contain no tryptophans and consist of two lysine terminal residues. The effect of adding the peptide to the membrane was inferred from changes in the oxygen relaxation of the spin-labeled lipid analogue. The present study is complementary in that the peptide itself was labeled and the oxygen profile measured, while Subczynski et al. measured the oxygen profile as seen from the perspective of the lipid. In the absence of any peptide, they observed an oxygen profile that is qualitatively similar to the one observed in these studies. The relaxation due to the oxygen in the interfacial region is around 1−1.5 Mrad/s, a value nearly the same as that which we obtained with the probe on the peptide. In the hydrophobic region, the relaxation rates were between 2 and 2.5 Mrad/s, which was somewhat lower than the values of around 3 Mrad/s reported here (see Table 2). It is somewhat surprising that the spin-labeled lipid, which presumably has more conformational freedom and hence increased dynamics, would show a decreased response to the oxygen in the hydrophobic region. The membrane-bound probes of Subczynski et al. give values that are about 25% smaller than the values reported from the peptide-bound probes in this

(47) Popp, C. A.; Hyde, J. S. *J. Magn. Reson.* **1981**, *43*, 249−258.
(48) Subczynski, W. K.; Lewis, A. H.; McElhaney, R. N.; Hodges, R. S.; Hyde, J. S.; Kusumi, A. *Biochemistry* **2001**, *40*, 12103−12111.

study using WALP. The two factors responsible for this difference are the relative diffusion coefficient and the local oxygen concentration. The other factor that warrants consideration is the nature of the lipid. In the present studies, DOPC was used. In the studies of Subczynski et al., POPC was used. To test the effect of the lipid, we carried out similar experiments using other membranes. Table 2 contains relaxation measurements at position 12 on WALP (in the middle of the membrane) for several bilayers. The values measured by Subczynski et al. for phosphatidylcholine spin labeled at position 16 in POPC at 20 °C are also given in Table 2. There is significant variation due to bilayer composition. Further comparison of the peptide-based probe (WALP) and the lipid-based probe of Subczynski et al. would require that the measurements be made on the same lipid system.

The sl-WALP relaxation profiles can be compared with the measurements of Subczynski et al. for the oxygen relaxation reported by spin-labeled phosphatidylcholine that is incorporated with peptide. The relaxation of spin-labeled phosphatidylcholine was measured with $(LA)_{12}$ and $(LL)_{12}$ at 10 mol %; which means there are five lipids (spin labeled or otherwise) on each side of the bilayer per peptide in these measurements. Essentially, there can be no peptide-free lipid in the experiments using spin-labeled phosphatidylcholine at these peptide concentrations. In contrast, the sl-WALP experiments were conducted with 1 mol %, so that there are 50 lipids on each side of the bilayer per peptide. The high peptide concentrations used in the study of Subczynski et al. ensure that the spin-labeled phosphatidylcholine lipids detect the relaxation effects of oxygen in the vicinity of the peptide. This parallels the fact that the experiments using sl-WALP must also be measuring the relaxation profile in the vicinity of the peptide. The finding from the spin-labeled phosphatidylcholine experiments of Subczynski et al. is that $(LL)_{12}$ caused no change in the relaxation profile of oxygen and that (in contrast) $(LA)_{12}$ reduced the relaxation rate in the hydrophobic region by 2-fold, so that the relaxation rate in the center of the bilayer was nearly the same as that in bulk. Subczynski et al. ascribe the effect of $(LA)_{12}$ to the different packing of POPC in the voids afforded by the alanine residues. The local protein environment for the spin probe is an ···L−A−slC−A−L··· unit contained within the sl-WALP. It is possible that POPC and DOPC are different in their organization in the vicinity of the peptide, and that the high concentration of peptide forces a packing order on the lipid for the experiments of Subczynski et al. Subczynski et al. argue that the lipid organization decreases the number of voids for oxygen, and this, in turn, decreases oxygen transport. Our experiments suggest that at a lipid-to-peptide ratio higher than that used by Subczynski et al., nothing noteworthy happens to the oxygen profile due to the presence of the (LA) repeat. Testing this suggestion requires measuring (or calculating) the effect of the lipid−protein interface on both oxygen concentration and dynamics.

In summary, the regularity of the nitroxide dynamics as a function of position in the membrane argues that there is nothing remarkable about the organization of the lipid against the WALP peptide. It is possible that the POPC, studied by others, will organize differently than the DOPC studied here. Subczynski et al. argue that the presence of $(LA)_{12}$ reduces the oxygen relaxivity by a factor of 2, but the peptide concentration was larger by an order of magnitude than the WALP concentration used in the present study. Our results give no indication of a reduced oxygen relaxivity in either DOPC or DOPM due to the presence of the LA repeat of the WALP peptide.

Comparison with Previous NMR Measurements of Oxygen Profiles. In complementary NMR studies, the paramagnetic property of oxygen was used as a relaxant of fluorine incorporated into proteins. In this recent work,[4] EPR methodology was criticized for lack of uniformity of probe response, limitations on oxygen concentration, and the inability to measure the spin−lattice relaxation rate directly. The present work address all three of these criticisms. Using pSR EPR, we are able to directly measure the spin−lattice relaxation rate using physiologically relevant concentrations of oxygen. If desired, the relaxation rates can be measured under a 5−10-fold increase in oxygen concentration. Unlike the ^{19}F NMR experiments, we are not constrained to operate at 100 atm of oxygen pressure. In summary, the EPR technique presented herein is complementary to NMR techniques and can be performed with 5 μL samples containing a probe at a concentration of 0.1 mM under physiological oxygen conditions.

Using the Oxygen Profile as a Ruler. The ΔR_1 relaxation profile obtained by the spin relaxant method is a product of two fundamental quantities: the local concentration of relaxant, which is an equilibrium property, and the diffusion rate, which is a transport property (see eqs 2 and 3, Materials and Methods). These two distributions that make up the relaxation profile cannot be disentangled using only the single relaxation profile. One approach is to abandon interpretation of a single relaxation profile and to use the ratio of oxygen and NiEDDA profiles. This strategy was first proposed by Altenbach et al.[12] and is based on the cancellation of the diffusion effect under the assumption that oxygen and NiEDDA have the same membrane transport parameters, thus leaving the ratio of concentration profiles (see Materials and Methods, eq 5). The original work suggested that this ratio parameter, Φ, depended linearly on membrane depth (see Figure 6). Equation 5 is applied to our data in Figure 6 and illustrates that there is significant deviation of Φ from linearity. The greatest nonlinearity occurs on the aqueous side of the Φ profile and resembles the form suggested by Cafiso and co-workers.[31] The Φ profile must achieve a plateau as the environment traverses to aqueous bulk conditions.

Even though the relaxation profile of a single relaxant contains both transport and equilibrium properties, such a profile is suitable for the determination of the depth of penetration of the nitroxide probe into the membrane bilayer. The relaxation profile is employed as a reference for spin labels attached to either transmembrane or peripheral membrane proteins for which depth of insertion data is desired. It has been a tacit hypothesis in all previous work, using spin-labeled *n*-doxyl stearic acid and transmembrane proteins, that the relaxation profiles measured by the membrane spin probes are still valid for nitroxide spin labels attached to the target proteins. A single α-helical peptide, WALP, is thought to be a more faithful model for the small loop regions of interfacial binding proteins than that of a large transmembrane multihelical protein.[4] The regular nature of the helix of the WALP peptide ensures that the peptide steric effects are the same for all residues. There are no steric conflicts with adjacent segments of the protein.

The oxygen (and nickel-based) profiles obtained from the WALP peptide are designed to calibrate the spin−lattice relaxation rates measured by pSR for a spin-labeled protein of

Table 3. Oxygen Exposure Factor (EF) Parameters Determined from CW Measurements Made on Mutants of cPLA2 C2 Domain on DOPM LUV (ref 37)

residue	EF[b]	depth	EF[c]	depth	depth[d]	depth[e]
V97 (CRB3)	2.27	12(2)[f]	2.4	13(2)	13	7
L39 (CRB1)	2.58	14(2)	2.4	13(2)	7.5	15
A34 (CRB1)	1.6	11(2)	1.7	11(2)	3	9
V70	0.9		0.86		−14	−17

[a] The depth is estimated from the DOPM calibration curve and compared with estimates made from similar residues from the study of the C2 domain in POPC/POPS (3:1). The depth is taken to be the distance from the phosphate headgroup toward the bilayer interior (in angstroms). Negative depth means out of the bilayer. [b] $EF = \Delta P_2^{+M}/\Delta P_2^{-M}$. [c] $EF = \{\Delta P_2^{+M}/\Delta P_2^{-M}\}\{P_2^{o-M}/P_2^{o+M}\}$. [d] Solution-exposed residue (V70) determined from the EPR technique in Ball et al.[37] [e] Estimated from Frazier et al.[31] [f] Errors are in parentheses, for example, 12(2) means 12 ± 2 Å.

interest bound to a membrane surface. Time domain data for such systems are still very limited in the literature.[9,21,29] The orientation of a secreted phospholipase A_2 was studied by pSR, but shows little penetration into the membrane.[21,49] Continuous wave studies using progressive saturation are extensive.[29,31,37,38,49] Two independent continuous wave EPR studies of the C2 domain of cytosolic phospholipase A_2 on different membranes confirm that two of the three calcium-binding loops of this protein domain penetrate into the membrane hydrophobic core.[31,37] The C2 domain is a good candidate for comparison of the different methods for obtaining the depth of insertion into the membrane. The C2 domain represents a conserved structural motif found in more than 50 proteins involved in lipid signaling, lipid metabolism, and vesicular trafficking. The C2 domain of cytosolic phospholipase A_2 has an important role in calcium-dependent transfer of the protein from the cytosol to internal cellular membranes as a prelude for arachidonate release from membrane phospholipids. The calcium-binding loops of the C2 domain, containing amino acid residues V34, L39, and V97, show increased oxygen relaxation, as a result of membrane binding (see Table 3).[31,37] Residues that are located away from the binding site show no oxygen relaxation enhancement upon membrane binding (V70, in Table 3, is an example). Figure 3S in the Supporting Information shows the orientation of the C2 domain on DOPM vesicles obtained using a solution-sequestered spin relaxant technique.[37] The hydrophobic interaction of the loops with the membrane is thought to be an important component in the driving force for the binding.[31,37,49] Oxygen data were reported in the later study, but were only analyzed qualitatively because of the lack of simultaneous NiEDDA data. The accuracy of the oxygen relaxation profile from the WALP ruler now enables direct use of oxygen data without recourse to a NiEDDA profile.

Recently, we compared CW EPR relaxation measurements to the analogous data determined using time domain (pSR) methods.[21] The comparisons show that there is difficulty in using any single conversion factor between the continuous wave and the time domain values; therefore, we present a simple, approximate comparison assuming that the CW data are only off by a proportionality constant from the time domain data. The exposure factor, defined as the ratio of oxygen relaxation of the spin-labeled protein bound to the membrane divided by the oxygen relaxation of the same spin-labeled protein in the absence of membrane, gives a simple number for comparison. The denominator of the exposure factor is included to account for the variation of the oxygen accessibility among labeling sites on the protein, due to local protein steric interactions. The proportionality constant between time domain and continuous wave exposure factors is taken to be 0.8 based upon our previous findings for oxygen relaxation of another protein system.[21] With this conversion constant, it is possible to use the data of Figure 5 to determine a depth from the CW-measured exposure factors (see Materials and Methods, and Supporting Information). The exposure factors and related depths are given in Table 3. A comparison is made with estimates of depth obtained previously by CW techniques.[31,37] Two different methods of analyzing the exposure factors from the CW data are show in Table 3 and give somewhat different estimates on the depth. The depth predicted by an independent EPR measurement that orients the protein on the membrane surface using solvent-exposed residues is also given in Table 3 (details are given elsewhere). It is clear that all methods predict that two regions of the C2 domain (designated CBR1 and CBR3) of cytosolic phospholipase A_2 have residues that are in the interior of the membrane (with depths more than 10 Å below the plane formed by the membrane phosphates).

Concluding Remarks

The primary result presented in this study is the introduction of a new spin-label ruler for measuring oxygen relaxation as a function of distance through the bilayer of membranes. The conventional methods in the literature rely heavily on the use of spin-labeled lipid analogues to measure the relaxation due to oxygen and other paramagnetic species in membranes. The continuous wave EPR spectra of these lipid analogues have shown increasing disorganization of the probe lipid as the labeling position approaches the center of the membrane bilayer.[11] Ideally, the probe lipid should be rigid so that the spin label at a given site is localized and accurately reports the local concentration of paramagnetic species. The spin-labeled peptide introduced in this study is a rigid α-helix that incorporates in the membrane with a known registration and is known to have a helical axis perpendicular to the membrane plane. The continuous wave and time domain EPR spectra are nearly uniform for all labeling positions of the peptide in the membrane, in contrast to lipid analogues.

Hubbell and co-workers introduced the use of spin-labeled transmembrane proteins to report oxygen and NiEDDA relaxation. Because the peptide used in these studies is a single α-helical peptide, synthesis was much easier than the mutagenesis techniques required to obtain a multihelical transmembrane protein. Moreover, the single α-helical WALP peptide may be labeled at all positions without steric interference, allowing a ruler with a higher density of calibrated positions. The WALP ruler requires only a single relaxant because the response of the spin labels is uniform along the full length of the peptide.

The collisional relaxation rate due to oxygen that is measured by EPR depends on two factors: the oxygen concentration in the vicinity of the spin label, and the diffusion rate of oxygen in the vicinity of the spin label. Theses two factors cannot be separated without a further experiment. However, the average of the relaxation rate over the entire bilayer can be factored into the average oxygen concentration and the average diffusion

(49) Canaan, S.; Nielsen, R.; Ghomashchi, F.; Gelb, M. H.; Robinson, B. H. *J. Biol. Chem.* **2002**, *277*, 30984−30990.

rate in the bilayer. Thus, the experimental data presented here suggest that the average diffusion coefficient for oxygen is between 2 and 10 times smaller in the membrane bilayer than that in water. The slower diffusion rate of oxygen found here is in agreement with current molecular dynamics studies, but there are conflicting predictions reported in the molecular dynamics literature.[27,28]

Even though oxygen relaxation depends on both concentration and diffusion, the membrane-depth-dependent profile of oxygen relaxation measured by the WALP peptide can be used as an empirical calibration for measuring the depth of other nitroxides in the same membrane. Oxygen data from the spin-labeled C2 domain of cytosolic phospholipase A_2 bound to a membrane surface were revisited, and the depth of insertion of residues on the calcium-binding loops of the C2 domain was quantified with the WALP ruler. The distances obtained are in good agreement with previous results from another EPR technique and an oxygen study using spin-labeled lipids. The registration of the C2 domain on the DOPM membranes places the two calcium ions that are bound to the C2 domain in proximity to phosphates of the phospholipids. Neutralization of the calcium partial charge by the phosphates may be a crucial component in the mechanism of calcium-mediated translocation of the cytosolic phospholipase A_2 enzyme to cellular membranes. Charge neutralization then presumably permits the two hydrophobic helical loops, CRB1 and CRB3, to penetrate the membrane and anchor the C2 domain to it. The two previous studies, as well as this one, concluded that both loops penetrate into the membrane (see Table 3). The study of Ball et al.[37] concluded that CRB3 was the primary binding loop, while that of Frazier et al.[31] concluded that CRB1 was the more deeply penetrating loop. This study shows that both loops penetrate to a similar depth and suggests an orientation intermediate between the two previous predictions.

Acknowledgment. This work was supported by Grants HL36235, HL50040, and GM065944 from the National Institutes of Health, and UW Environmental Sciences Center Grant P30-ESO7033 from NIEHS. The authors wish to acknowledge helpful discussions with Drs. J.A. Killian and S. White, and wish to thank Dr. White for kindly providing us with the probability profiles in Figure 1.

Supporting Information Available: Approximations necessary for separation of equilibrium and transport parameters using the relaxation gradient. Table 1S: line width and spin−lattice relaxation data for WALP in DOPC. Table 2S: line width and spin−lattice relaxation data for WALP in DOPM. Table 3S: Least-squares fitting parameters for relaxation profiles. Figure 1S: CD spectra WALP23-12 DOPC/DOPM. Figure 2S: CW EPR spectra, WALP in DOPM. This material is available free of charge via the Internet at http://pubs.acs.org.

JA042782S